Journal of Structural Geology, Vol. 9, No. 5/6, pp. 705 to 717, 1987
Printed in Great Britain

0191-8141/87 $03.00 + 0.00

A 3-D kinematic model of fabric development in polycrystalline aggregates: comparisons with experimental and natural examples

A. ETCHECOPAR

Laboratoire de Géologie Structurale—U.S.T.L.—Place E. Bataillon—34060 Montpellier Cédex, France

and

G. VASSEUR

Centre Géologique et Géophysique—U.S.T.L.—Place E. Bataillon—34060 Montpellier Cédex, France

(*Received* 10 *March* 1986; *accepted in revised form* 6 *March* 1987)

Abstract—A 3-D generalization of the approach previously developed by Etchecopar for the simulation of fabrics in polycrystalline aggregates is presented. The model is based on a geometric minimization of gaps, overlaps and boundary displacements between deformed neighbouring cells; each cell may deform using a small number (<5) of independent slip systems. The model is applied to experimentally flattened peridotites and sheared ice as well as to naturally sheared peridotites and quartzites. For weak deformations, the simulation matches the natural and experimental observations but, for large deformations, major discrepancies are observed; in particular the model cannot explain the obliquity of Lattice Preferred Orientation with respect to the schistosity, which is commonly observed in shear deformations. However, when taking into account a 'dynamic recrystallization' process, these discrepancies are strongly reduced and the obliquity clearly appears in simple-shear models.

INTRODUCTION

SINCE THE work of Nicolas *et al.* (1971) on peridotites, the analysis of Lattice Preferred Orientations (LPO) is commonly used for the kinematic interpretation of plastic deformation. It is widely accepted that the obliquity of LPO of quartz or olivine with respect to schistosity or foliation (XY plane) is an expression of rotational deformation and can be used to determine the sense of shear. Systematic observations in shear zones support this assumption (Kojima & Hide 1958, Laurent & Etchecopar 1976, Hudleston 1977, Mattauer *et al.* 1977, Burg & Laurent 1978, Brunel 1980, Prinzhofer & Nicolas 1980, Malavieille & Etchecopar 1981, Garcia Celma 1983). However, this criterion remains qualitative because of the difficulty of performing experimental shear deformation on natural samples. For this reason, numerical simulations seem very attractive.

Following the analysis of Bishop & Hill (1951), Lister *et al.* (1978) proposed a numerical simulation for polycrystalline deformation based on an energy criterion. Their model assumes that a homogeneous deformation occurs throughout the polycrystalline aggregate and that each crystal must achieve the imposed deformation through various slip systems. It can be shown (Von Mises 1928) that at least five independent slip systems, each resulting in a simple shear deformation, are required to achieve a given bulk homogeneous strain. Some of Lister's models (e.g. models A and C of Lister & Hobbs, 1980) agree well with LPO diagrams of experimentally flattened quartzites (Tullis *et al.* 1973).

However, this model cannot be applied to crystals where only a few glide systems exist (e.g. olivine and ice) because a homogeneous deformation is then impossible to achieve. In the case of low-temperature shear deformation of quartzite, this model can hardly predict the observed obliquity between the actual LPO and the schistosity (Marjoribanks 1976, Bouchez 1977). For example, model C of Lister & Hobbs (1980, fig. 14) predicts the correct asymmetry in the rose diagram of the trend of c-axis in the XZ plane; however, the asymmetry in the c-axis pole figure remains quite weak even after 60% shortening.

Various observations in peridotites show that strain is very heterogeneous from one crystal to the next (Boullier & Nicolas 1973). In order to allow such a heterogeneous deformation, other mechanisms such as recrystallization must necessarily take place. The importance of recrystallization in natural deformation is well known (Carter *et al.* 1964, Nicolas & Poirier 1976, Urai *et al.* 1986) and this process should be included in realistic models.

In this paper, we propose an alternative approach based on purely geometric considerations; this approach is the 3-D generalization of a model previously developed in 2-D (Etchecopar 1977). The basic principle of this method is to restrict the slip systems to those which are well documented; in most rocks, and especially in peridotites, this number is less than five. Therefore each crystal cannot match exactly the imposed deformation. Since the deformation of neighbouring crystals may not be the same, gaps, overlaps and grain-boundary sliding necessarily occur. The proposed method consists of an iterative minimization of these gaps, overlaps and also boundary sliding between crystals. As long as gaps and overlaps remain weak, we

assume that they can be absorbed by other physical mechanisms such as diffusion, recrystallization, flexuring, twisting, etc.

We first describe the method used, then test the results for coaxial straining with data obtained on experimentally flattened dunite by Nicolas *et al.* (1973). Next, we consider shear strain; in this case, the model indicates that, for large strains, gaps and overlaps increase drastically whereas the fabrics remains symmetric. We then propose a numerical procedure which simulates a recrystallization process. LPOs produced by a combination of slip and recrystallization are in good agreement with natural ones. In particular, progressive shearing yields oblique fabric patterns.

METHOD

Initial aggregate of cells

The assumed aggregate is an array of 216 (6 × 6 × 6) cells, identical in shape, and filling the whole space. Each cell is a regular polyhedron shown in Fig. 1 with 14 vertices, 24 edges and 12 faces; such a geometry was chosen in order to limit anisotropy effects during the interaction between the various cells. The initial lattice orientation of each cell is chosen through a random orientation of its reference axes. Each slip system consists of a slip plane, defined by its normal, and a slip direction belonging to that plane. Up to five independent glide systems can be used. In fact we restrict the simulation to one, two or four independent glide systems, intended to simulate olivine, ice and quartz deformation.

Simulation method

In order to achieve a finite deformation, we proceed through two imbricated iterative loops. The first loop consists of an incremental deformation of the envelope of the aggregate; the increment of each step is $\Delta\gamma = 0.2$ for shear strain and 10% shortening for coaxial flattening. For each increment of strain, the second loop achieves the deformation of each cell and computes its internal rotation and slips according to the iterative procedure described below, and illustrated in Fig. 2.

When a strain increment—either coaxial flattening or simple shearing—is applied to the external envelope, we first define an ideal deformed array as a result of a homogeneous deformation (dotted lines of Fig. 2b). In fact, a given cell cannot achieve exactly this deformation due to its limited number of slip systems; nevertheless, we can obtain, for each cell, the kinematic parameters—rotation, translation and slip—such that the deformed cell approaches this geometry as close as possible. The best fit is obtained by minimization of the quadratic sum:

$$q = \sum_{i=1}^{14} [(X_i - X_{ti})^2 + (Y_i - Y_{ti})^2 + (Z_i - Z_{ti})^2],$$

(X_i, Y_i, Z_i) being the actual co-ordinates of the vertices of the deformed cell and (X_{ti}, Y_{ti}, Z_{ti}) being those of the ideal cell. For small deformations, q depends quadratically on the rotation, translation and slip parameters which can therefore be obtained directly by matrix inversion.

When this is done successively for each cell, a new array of cells is obtained with relatively large gaps and overlaps (solid lines in Fig. 2b). In order to take into account the interaction between neighbouring cells, a new ideal array is defined. Each vertex of this ideal array corresponds to the barycenter of vertices initially belonging to neighbouring cells, as shown in Fig. 2(c). In

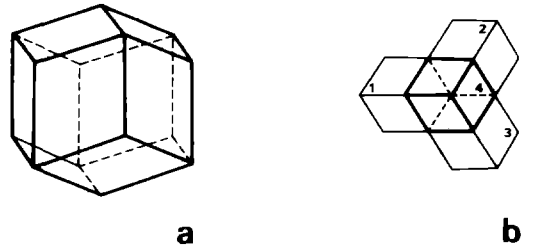

Fig. 1(a). Geometry of the elementary cell (polyhedron with 14 vertices). (b) Assembling of four elementary cells simulating a part of the aggregate.

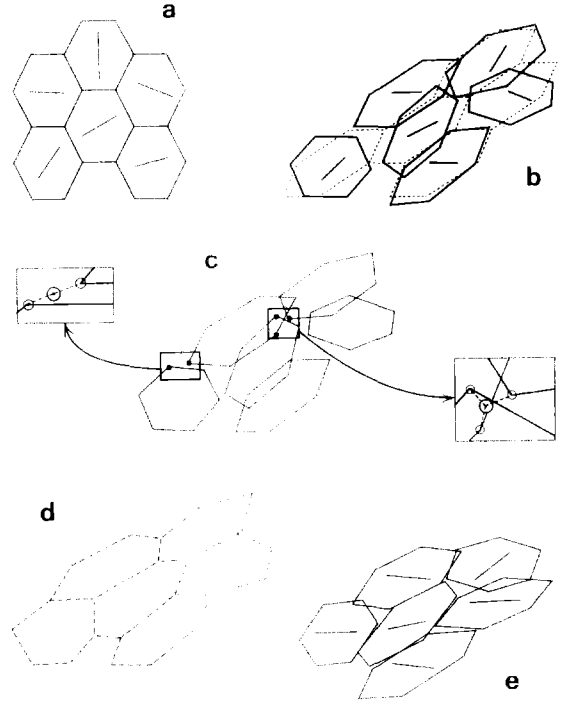

Fig. 2. Illustration of various steps of the simulation. (a) Initial aggregate before deformation. Dashes represent the projection of the slip plane. (b) Dotted lines represent the ideal shape of the model aggregate that we should obtain through a homogeneous simple-shear deformation; solid lines are the shapes actually obtained at the first iteration, using best estimate of rotation, translation and slip parameters. (c) At this step, actual cells are disjointed. Barycenters of vertices, initially belonging to neighbouring cells are then defined. (Details shown in insets.) (d) Using these barycenters, a new ideal model aggregate of cells is defined. In the following iteration, each cell tries to achieve the corresponding shape. (e) As a result of the next iteration, a new geometry of cells is obtained. Note that gaps and overlaps remain but are smaller than in (b). The processes described in (c)–(e) are then iterated until the geometry does not change any longer.

order to approach this new array (Fig. 2d), the kinematic parameters giving the best fit between actual vertices and ideal vertices are computed. The same minimization criterion is used; this time (X_{ti}, Y_{ti}, Z_{ti}) are the co-ordinates of the barycenters previously defined.

The resulting array of cells shown in Fig. 2(e) presents smaller gaps and overlaps. This process of barycenter definition and parameter optimization for all cells is iterated until q does not decrease any longer, for any cell.

This simple procedure, similar to that used by Etchecopar (1977), does not explicitly deal with volumetric gaps and overlaps; however it has the advantage of minimizing the cell boundary sliding. Moreover, the algorithm is very simple and, as shown later, the simulation generally gives acceptable gaps and overlaps.

COAXIAL FLATTENING: COMPARISON WITH EXPERIMENTALLY DEFORMED PERIDOTITE

In order to test the model we compare our results with those obtained by Nicolas *et al.* (1973) on synthetic dunite experimentally deformed by coaxial flattening. In this case, one slip system (0 1 0) [1 0 0] is largely predominant; therefore, it was the only one that we considered at first. For each cell this system is defined by the normal N to the glide plane, the slip direction G and an auxiliary direction A (see Fig. 3).

The flattening of the aggregate is simulated by applying successive shortening increments of 10%. The resulting distribution of each axis is shown in Fig. 4 for the initial stage and for shortening of 36, 49 and 65%. For the final stage (65% shortening) the volumetric gaps and overlaps reach about 15% of the total volume. Starting from a rather homogeneous initial fabric, two of the axes clearly exhibit a reorientation: the axis N (normal to the slip plane) tends toward the shortening direction with a relative density minimum in this direction; the distribution of the axis G (slip direction) forms two girdles, approaching the flattening plane with increasing shortening strain. However the auxiliary axis (A) does not exhibit any clear preferred orientation.

These results are in good agreement with the experimental data of Nicolas *et al.* (1973) (Fig. 5) for the reorientation of the two axes N and G; however, for a given strain, the orientation is more pronounced for the experimental fabrics than for the simulated ones. Furthermore the third axis A exhibits a distinct reorientation in the experiment but only a weak preferred orientation in the model.

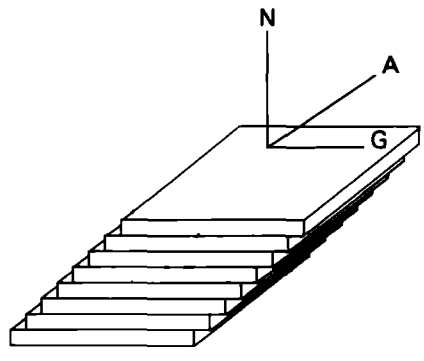

Fig. 3. Reference frame of an individual cell. G is the slip direction in the plane normal to N. A is an auxiliary direction.

This latter discrepancy may be due to the existence of a secondary slip system with the same slip plane and with A as the slip direction. Thus we attempted a new simulation in which, for each strain increment, this second slip system—(0 1 0) [0 0 1]—is only allowed, once the minimization is completed with the first system alone. In this case, the new diagrams (Fig. 6) are very similar to the previous one with respect to the N and G axes but they now exhibit a preferred orientation for the A axis, which is in better agreement with the experimental data.

THE CASE OF SIMPLE SHEAR—COMPARISON WITH EXPERIMENTALLY DEFORMED ICE

Experimental data on rocks deformed in simple shear are not presently available. Yet torsion experiments on ice provide interesting results since the slip systems of ice are similar to those of quartz (i.e. basal). The plastic deformation of ice uses six slip directions normal to the c-axis (i.e. in the basal plane). For the simulation, we use only two independent orthogonal slip directions, any other being achieved by some linear combination of these. The shear of the aggregate is simulated with a shear increment $\Delta\gamma = 0.2$ until a maximum total shear of $\gamma = 3$ is reached. For γ less than 2, the volumetric ratio of gaps and overlaps with respect to the initial volume remains low (<10%) but it increases dramatically for γ larger than 2.

Starting from a homogeneous initial fabric, Fig. 7(a) shows the development of a preferred orientation for the axis N normal to the slip plane (equivalent to the c-axis of ice). The distribution of the N axis is clearly bimodal: most axes occur along two crossed girdles, one being normal to the shear plane, the other being its mirror-symmetry image with respect to the XY plane. The maximum concentration in each girdle is in the outer region of the diagram.

This distribution is very similar to that obtained by Lister & Hobbs (1980) in the case of quartz with relatively easy basal glide. A comparison with the experimental data on ice of Bouchez & Duval (1982) (Fig. 7b) reveals some similarities but also striking differences. For low strain, the LPO experimental diagram exhibits two maxima with same overall orientations as in the simulation; but the experimentally produced maxima are much more concentrated in the outer region of the diagram and, even for low strain, the experimental fabrics are more pronounced. More important still, one of the maxima disappears for large experimental strain, something which does not occur in the simulation. Clearly, our model with slip as a fundamental deformation mechanism cannot explain the observation of asymmetric fabrics; other physical mechanisms must occur and are discussed below.

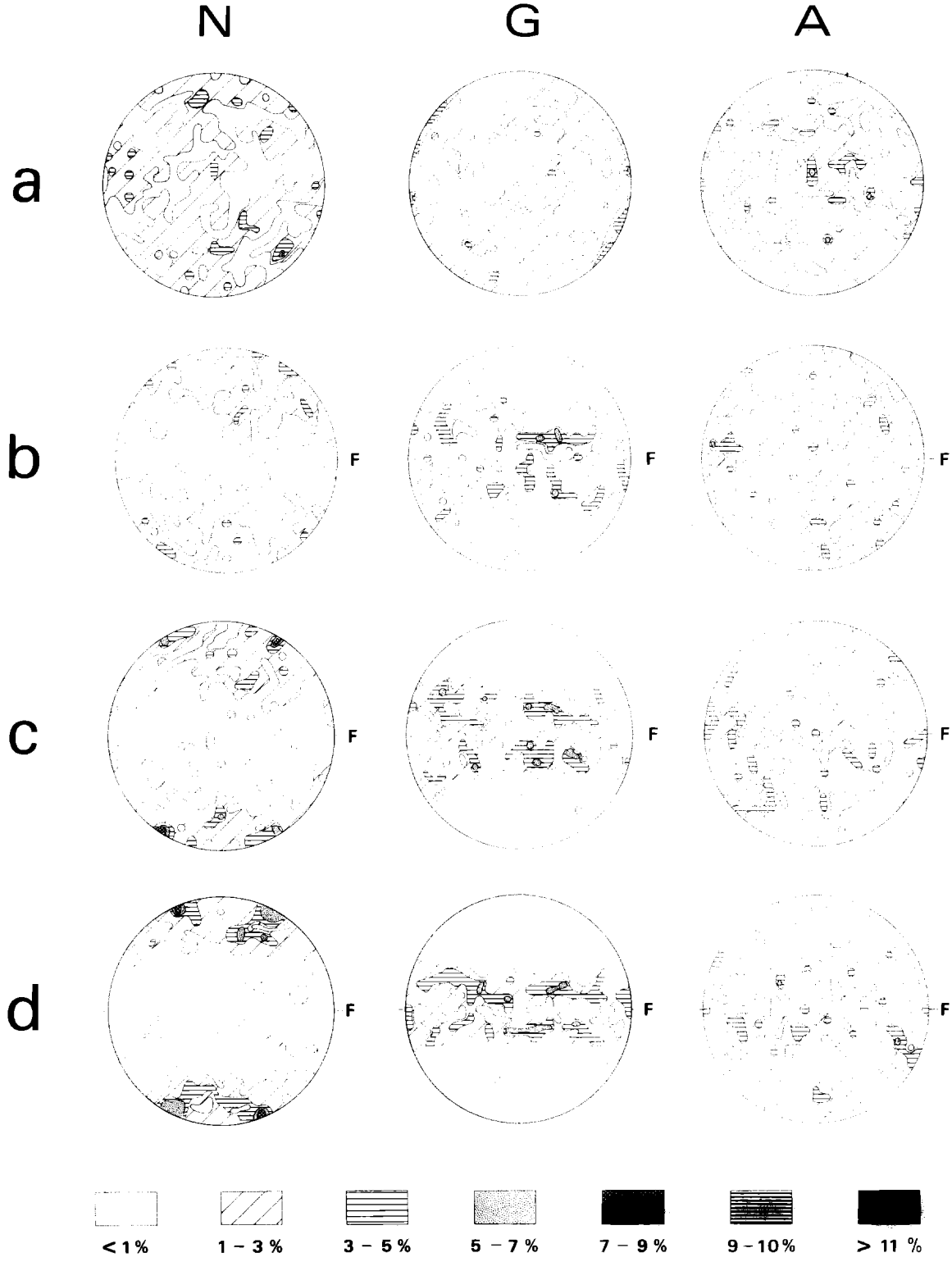

Fig. 4. Simulation of LPO for flattened peridotites (one slip system only: (010)[100]). For each axis, N [010], G [100], A [001] (cf. Fig. 3), the distribution is given for 216 cells in Schmitt projection as isodensity contours. Contours are for 1, 3, 5, 7, 9 and 11%. The horizontal line (F) is the projection of the flattening plane. (a) Initial model with no deformation; (b)–(d) are for 36, 49 and 65% shortening, respectively.

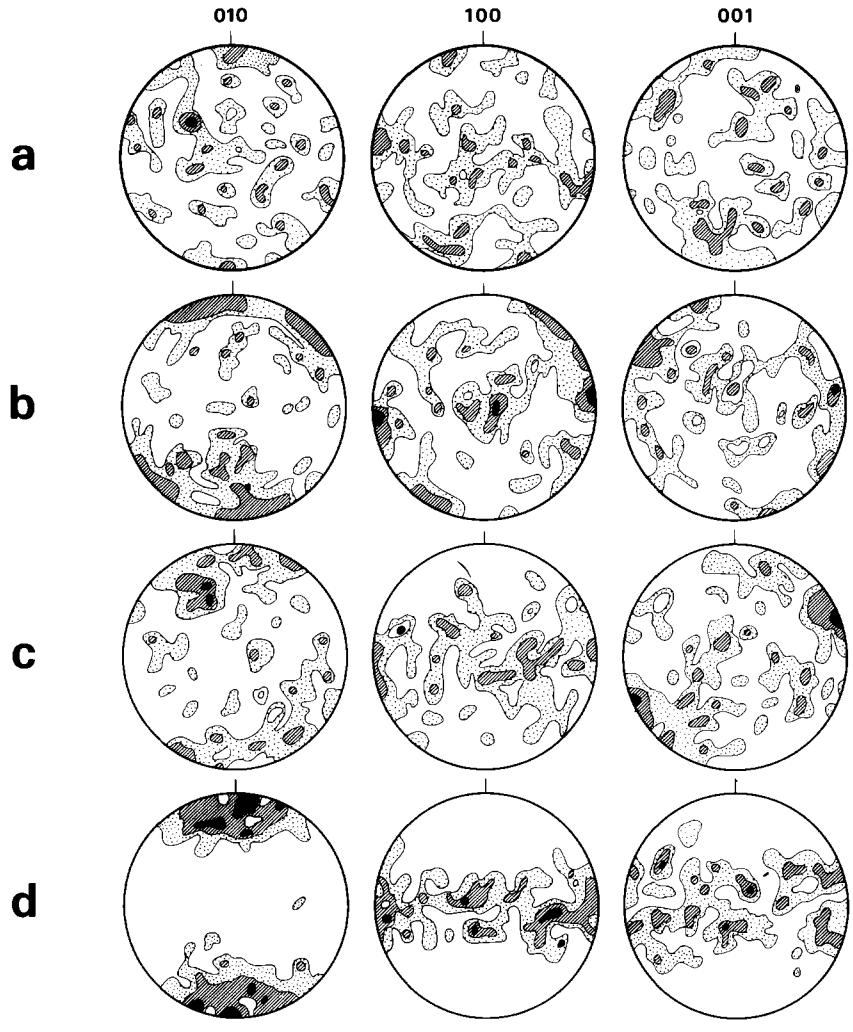

Fig. 5. Lattice Preferred Orientations obtained by Nicolas *et al.* (1973) for experimentally flattened synthetic dunites. One hundred crystals were measured and the LPO of the three axes (010, 100, 001) corresponding to *N*, *G* and *A* (Fig. 3) are given as isodensity contours for 2, 4 and 8%. (a) Initial distribution with no deformation; (b)–(d) are experimental distributions for 33, 44 and 58% shortening, respectively.

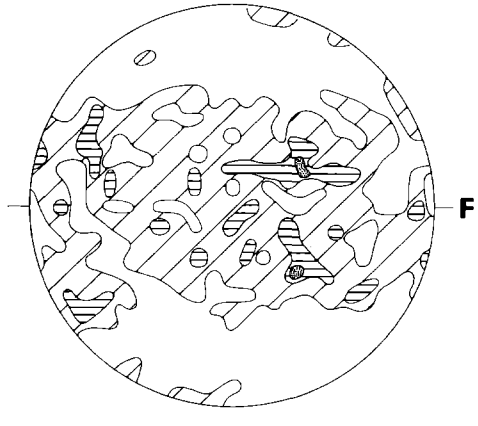

Fig. 6. Simulation of *A* axis distribution for flattened peridotites when allowing a second slip direction (*A*) in the *GA* plane (Fig. 3). Results are shown for 65% shortening. Symbols as in Fig. 4.

In order to explain the computed bimodal distribution of the LPO, it is interesting to follow the behaviour of each cell during the deformation process. This is much more easy to follow in the case of the 2-D simulation (Etchecopar 1977) where a similar bimodal distribution occurs. In this case, the cells can be separated into two sets according to the direction of the slip plane with respect to the shear direction, as illustrated in Fig. 8. These two sets correspond to the two maxima of the bimodal fabrics. For a cell of the first set, internal slip occurs in accordance with the imposed shear; the slip direction tends to become parallel to the shear direction and large cell deformations may occur easily. In contrast, cells of the second set are characterized by an internal slip opposite to the imposed shear; the modelled deformation of these cells results in more and more grain-boundary sliding. The cells of this second set become locked. Their deformation decreases and subsequent gaps, overlaps and grain-boundary sliding with neighbouring cells increase dramatically.

It seems likely that in the 3-D case the same situation occurs, when only one slip system is dominant. Such a

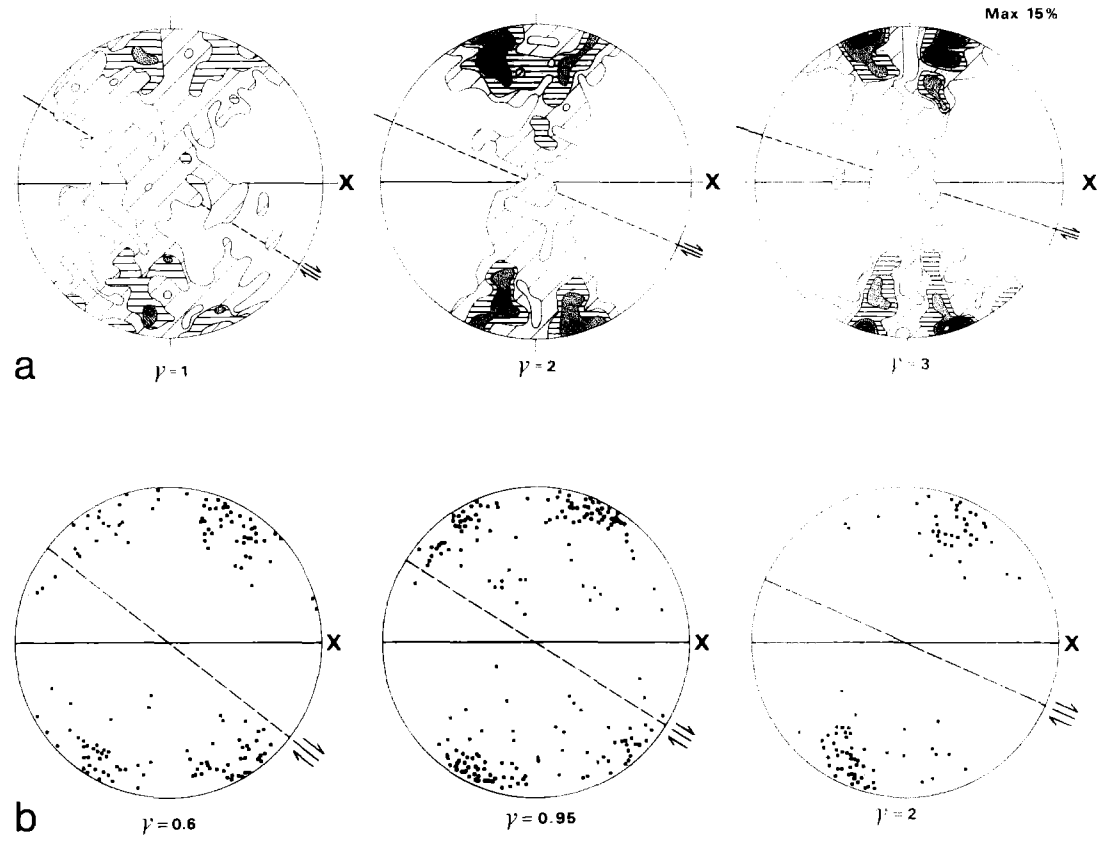

Fig. 7(a). Distribution of c-axis for the simulation of sheared ice. Isodensity contours correspond to 1, 3, 5, 7, 9 and 11%. The horizontal line (X) represents the projection of the XY plane and the dashed oblique line is the projection of the shear plane. Diagrams correspond to $\gamma = 1$, 2 and 3. (b) Distribution of c-axis in experimentally sheared ice from Bouchez & Duval (1982). Dashed line is the projection of the shear plane and line (X) is the projection of the XY plane. Diagrams are for $\gamma = 0.6$, 0.95 and 2.

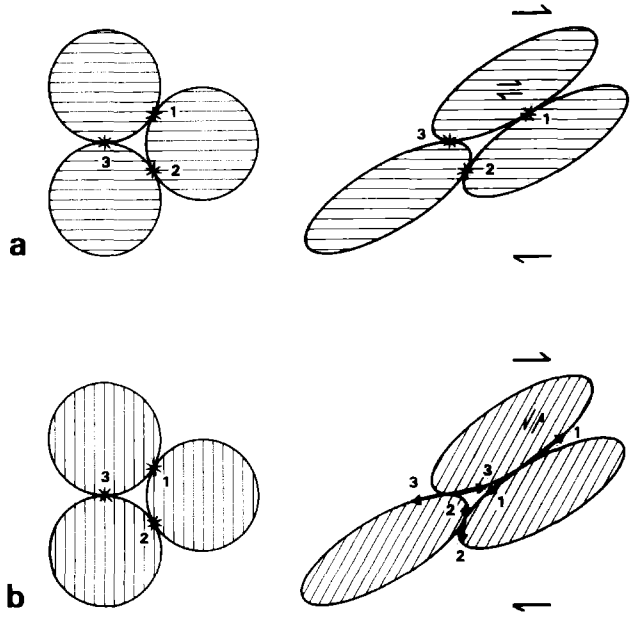

Fig. 8. Illustration of the behaviour of cells in the 2-D case showing how they can be separated into two sets according to the slip plane orientation (arrows). An initial circular shape is assumed. (a) Cells of the first set can achieve the imposed deformation by slip. Points initially belonging to neighbouring cells (1, 2, 3) remain adjacent after the deformation. (No grain boundary sliding occurs.) (b) For cells of the second set, the same imposed deformation results in large grain boundary sliding (points initially belonging to neighbouring cells become separated).

separation of cells into two sets is consistent with the observed and computed bimodal distribution of the LPO: the maximum normal to the shear plane corresponds to the cells of the first set, whereas the other maximum (oblique with respect to the shear plane) corresponds to the locked cells of the second set.

In natural aggregates, the locked cells obviously disappear after large deformations; this is true for experimentally and naturally deformed ice (Bouchez & Duval 1982, Hudleston 1977) and also for naturally deformed peridotites (Prinzhofer & Nicolas 1980) and low temperature quartzites (Bouchez 1977, Bouchez *et al.* 1982). In all these cases, the LPO diagrams exhibit only one maximum normal to the shear plane after large deformation. The important problem is therefore to find the physical processes which can explain the unlocking of the locked cells.

In natural rocks, two remarkable examples of unlocking can be observed; the first one is 'en cornue' crystals in which flexuring and twisting allow a progressive unlocking of part of the crystal (Etchecopar 1977). This results in a very characteristic shape as shown on Fig. 9. The second example is illustrated by the truncated enstatite crystals observed by Nicolas *et al*, (1971). In this case, the fracturing of a locked crystal normal to its elongation gives smaller and more isodiametric crystals which enables rotation favouring further slip in accor-

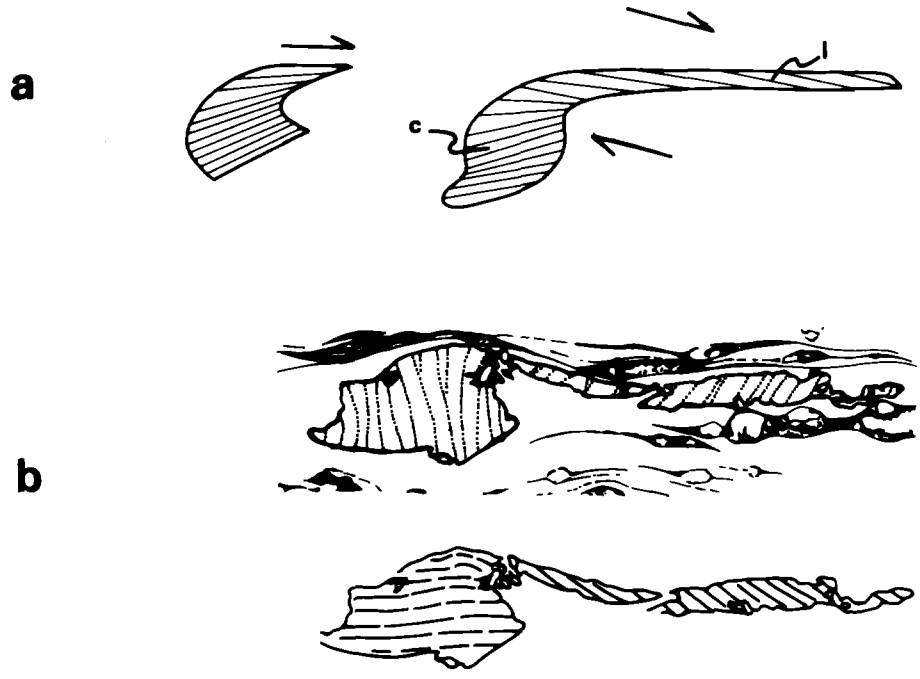

Fig. 9. Example of an 'en cornue' crystal. (a) Principle of the deformation: c is the locked part of the crystal and l is the part which forms the tail. (b) Natural example of 'en cornue' olivine crystal from Boullier & Nicolas (1973). The dotted lines correspond to dislocation walls and the lower figure displays the slip-plane directions.

dance with the imposed shear (Fig. 10). Although spectacular, these two mechanisms are obviously not the common way of unlocking.

A classical observation on naturally sheared rocks is that individual grains have a smaller elongation ratio (X/Z) than predicted by the estimated finite strain, especially, for large strains. Various authors (Carter *et al.* 1964, Hobbs 1968) explain this difference by dynamic recrystallization processes. Two recrystallization processes are currently accepted: recrystallization by grain-boundary migration, and recrystallization due to subgrain rotation (Hobbs 1968, Green *et al.* 1970, Tullis *et al.* 1973, Nicolas & Poirier 1976). Another classical observation in quartz ribbons is that the mean long axis of crystals is oblique with respect to the schistosity; such an example is shown on Fig. 11. It is interpreted by Brunel (1980) as a consequence of dynamic recrystallization.

With respect to Lattice Preferred Orientations, the major effect of such recrystallization processes is comparable to the cutting up of enstatite crystals: for a given crystal, recrystallization restores a more isodiametric shape and allows unlocking and rotation. Crystals for which the initial orientation was unfavourable can then be gradually reorientated so that their slip plane becomes parallel to the shear plane. The LPO distribution tends to be unimodal by removal of the maximum which is oblique to the shear plane. Such a relationship between the occurrence of LPO asymmetry and the amount of recrystallization is actually observed in quartz mylonites. Recently published data, obtained in the Moine Thrust zone (Law *et al.* 1986) are shown in Fig. 12. Away from the thrust plane, the old flattened grains present a symmetrical *c*-axis distribution whereas the *c*-axis distribution of surrounding recrystallized grains tends to exhibit a single girdle. It seems likely that these features are due to an increasing shear strain in the vicinity of the thrust plane. However, these observations could alternatively be explained in terms of a strain path dependence on the distance from the thrust plane (Law *et al.* 1986).

It is very difficult to model realistically such recrystallization processes. Therefore we designed a very rough way of taking them into account. We assume that when gaps, overlaps and grain-boundary sliding remain important once the minimization procedure is achieved, then each cell suddenly recovers its polyhedral shape with preservation of its last lattice orientation. Although this approach is very crude, it simulates the observed LPO quite satisfactorily.

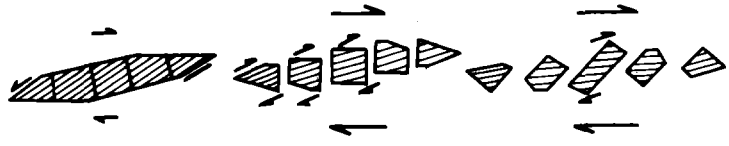

Fig. 10. Illustration of unlocking of a deformed locked crystal by fracturing into more isodiametric crystals and rigid rotation of the individual fragments.

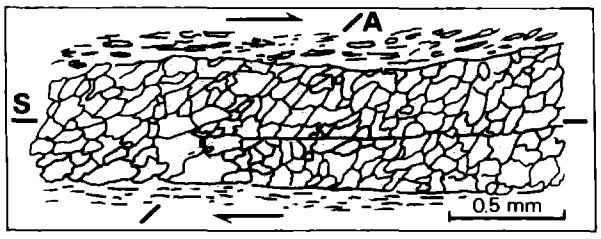

Fig. 11. Quartz ribbon parallel to schistosity showing quartz grains oblique (A) with respect to schistosity plane (S). This pattern is interpreted as due to dynamic recrystallization during shear deformation.

We now simulate the simple shearing of ice assuming that 'complete recrystallization' occurs for $\gamma = 2$ and $\gamma = 4$. Figure 13 illustrates the distribution of c-axes for high values of γ ($\gamma = 3$, 4 and 5). For $\gamma = 3$, a comparison with Fig. 7 (without recrystallization) shows an obvious difference: the LPO distribution now exhibits only one girdle, slightly oblique with respect to the XY plane, instead of two symmetric crossed girdles (Fig. 7a). For larger strain ($\gamma = 4$ and 5), these maxima become sharper and occur roughly normal to the shear plane. This unimodal distribution, oblique with respect to the XY plane, compares well with the LPO distribution of experimentally deformed ice for large strain (Fig. 7b).

The same model can also be applied to low-temperature quartz deformation for which the main slip systems are similar to those of ice. It is well known that, in sheared rocks, quartz exhibits LPO diagrams with a maximum oblique to the schistosity (Marjoribanks 1976, Bouchez 1977, Mattauer *et al.* 1977, Burg & Laurent 1978, Brunel 1980, Simpson 1980, Gapais & White 1982). Our results suggest that this feature is due to the combined action of shear deformation and recrystallization.

SIMULATION OF SIMPLE SHEAR IN PERIDOTITES

Natural examples of sheared peridotites are very scarce; nevertheless, Prinzhofer & Nicolas (1980) have studied a shear zone in harzburgites of New Caledonia. Their experimental LPO distribution of three axes of olivine crystals are shown in Fig. 14. These three axes ([0 1 0], [1 0 0], [0 0 1]) exhibit an intense fabric, particularly the first two.

The simulation assumes only one slip system, the one previously selected for the simulation of coaxial flattening of dunite. The computed LPO diagram of the three equivalent directions (N, G, A, cf. Fig. 3) are shown in Fig. 15 for a shear strain $\gamma = 5$, achieved with two 'complete recrystallization cycles' after $\gamma = 2$ and $\gamma = 4$. For the two first axes, the comparison is quite acceptable, in particular, in terms of their obliquity with respect to the schistosity. However, the distribution of the third axis does not exhibit clear fabrics. We thus proceeded again to a new simulation in which the second slip system of the same plane is allowed once the minimization is completed by slip on the first system. The resulting LPO diagrams are shown on Fig. 16; the maximum of the first axis distribution is strengthened whereas a weak fabric appears on the third axes. Differences with the observational results remain; they could be due to the existence of other slip systems and eventually to the fact that the actual strain path may differ from simple shear.

SIMULATION OF QUARTZ DEFORMATION WITH BASAL AND PRISMATIC SYSTEMS

At high temperature quartz deforms preferentially using both three basal and three prismatic slip systems

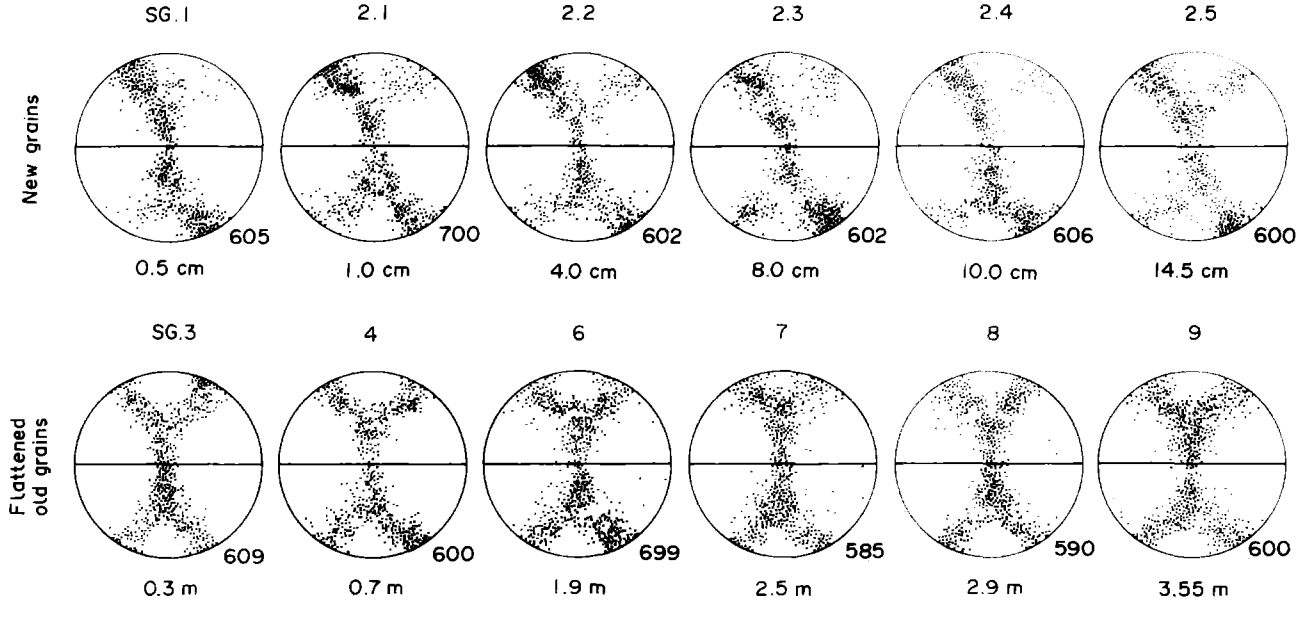

Fig. 12. Quartz c-axis fabrics from mylonitic Cambrian quartzites at the Stack of Glencoul, after Law *et al.* (1986, fig. 5). Distances from the Moine Thrust plane are indicated. The upper row are new (recrystallized) grains in the vicinity of the thrust plane; the lower row are old grains.

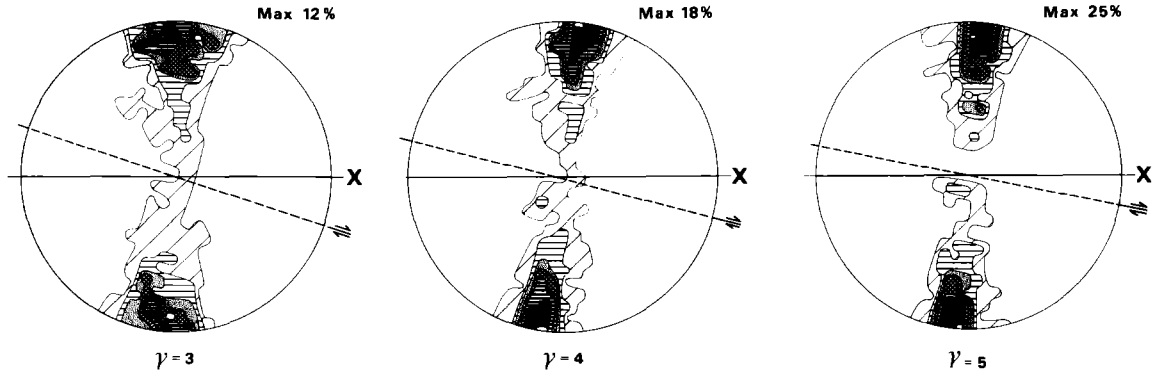

Fig. 13. Distribution of *c*-axis for the simulation of sheared ice. Two 'complete recrystallization' processes are performed for $\gamma = 2$ and 4. Diagrams are for a total deformation $\gamma = 3, 4$ and 5. Symbols as in Fig. 7(a). Max indicates the maximum density obtained.

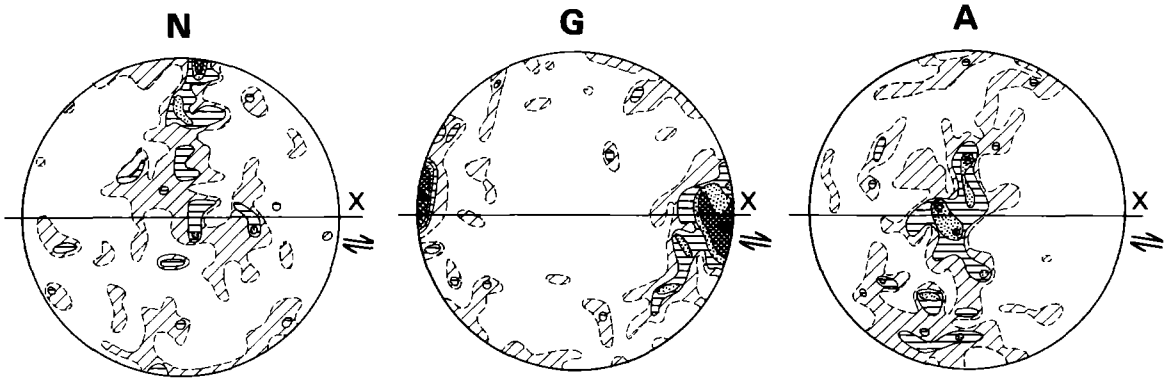

Fig. 14. Example of natural LPO distribution in harzburgite from New Caledonia (Prinzhofer & Nicolas 1980). One hundred crystals are measured for *N* [010], *G* [100] and *A* [001] axes. Isodensity contours are given for 1% (broken line), 3, 4, 6, 8 and 10%.

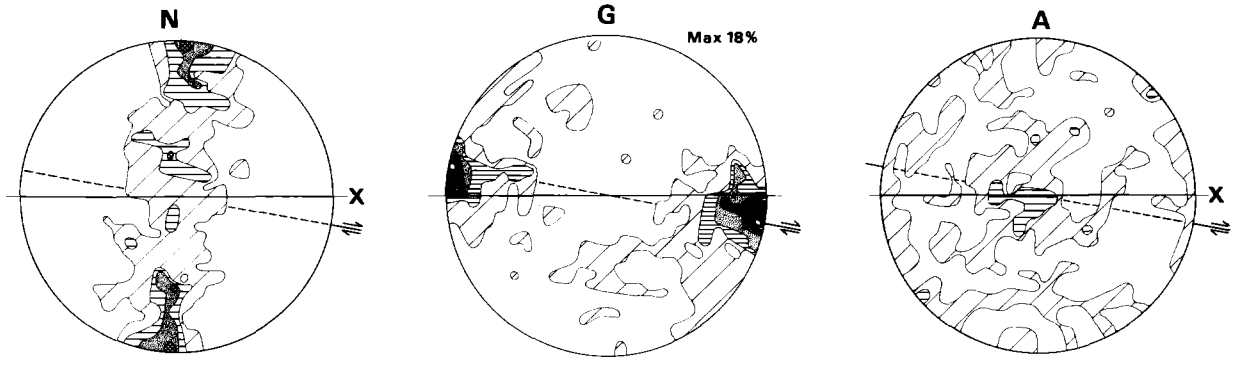

Fig. 15. Simulation of simple shear in olivine with one slip system, for $\gamma = 5$. Distribution of the three axes *N*, *G*, and *A* is given with isodensity contours for 1, 3, 5, 7, 9 and 11%. Max indicates the maximum density obtained.

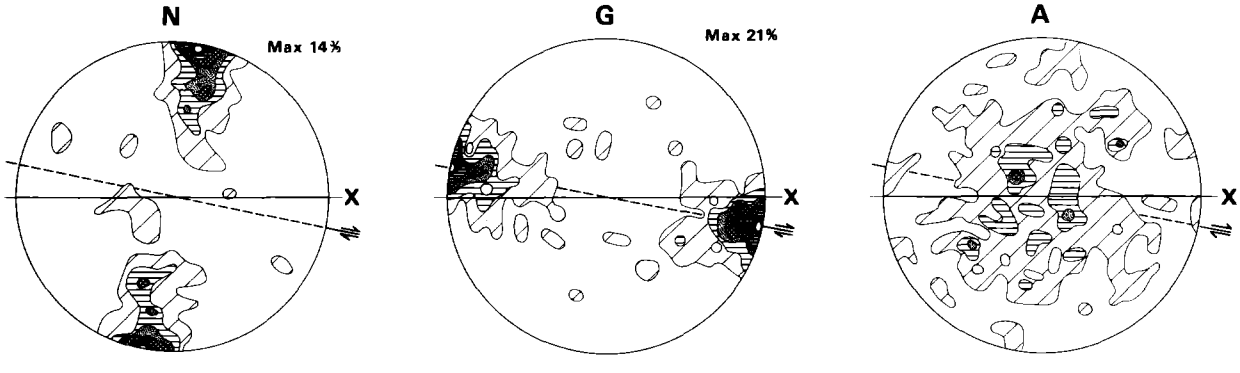

Fig. 16. Simulation of simple shear in olivine assuming another secondary glide system in the basal plane. All other details as for Fig. 15 caption.

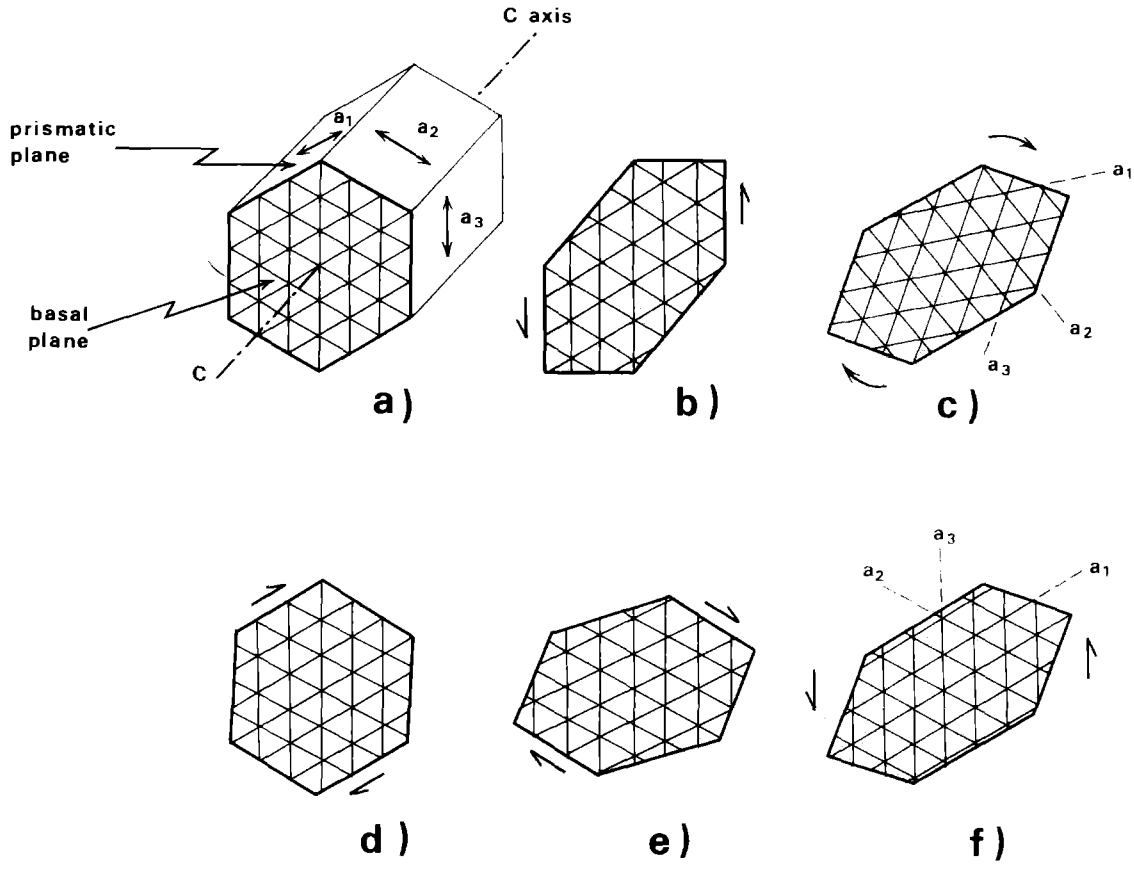

Fig. 17. (a) Sketch of a quartz crystal showing its three prismatic slip planes with their three slip directions (a_1, a_2, a_3) and their trace in the basal plane. (b)–(c) and (d)–(f) show two strain paths yielding the same overall deformation (c) and (f). The upper path (b, c) consists in a slip along a_3 followed by a rigid rotation. The lower path (d, e, f) consists in three slips along a_1, a_2 and a_3 without any rotation.

(Fig. 17a) (Nicolas & Poirier 1976). Of these six slip systems, only four are linearly independent. Moreover, in this case, the rotation around the *c*-axis is completely undefined; this is because the same crystal deformation can be achieved through different strain paths using the various prismatic slip systems, as illustrated in Figs. 17(b) & (c) and (d)–(f).

Since the kinematic parameters of each cell are chosen in order to optimize geometric criteria, no priority of any slip system with respect to the others was considered. This assumption is restrictive since the energy thresholds are certainly different for each slip system. However, as shown later, the general pattern obtained with this simple model is comparable with observations.

The results of the simulation of simple shear deformation are illustrated in Fig. 18 for γ varying from 1 to 5. For low values of γ ($\gamma \leqq 2$) the *c*-axes are concentrated in two small circles, symmetrical with respect to the *XY* plane. For high values of γ, most *c*-axes lie on a single girdle, oblique to the *XY* plane. The maxima of the distribution are located nearly 25° from the *XZ* plane. In this simulation, two 'complete recrystallizations cycles' were assumed for $\gamma = 2$ and $\gamma = 4$; but in the present case, the recrystallization is not of major importance: due to the four independent slip systems, any cell can easily achieve the imposed deformation and no serious locking occurs.

Numerous natural data of LPO distribution in high-temperature deformed quartz are available (Kojima & Hide 1958, Bouchez & Pecher 1976, 1981, Bouchez 1977, Brunel 1983, Simpson & Schmid 1983, Garcia Celma 1983). Two examples are given in Fig. 19. It seems that the proposed model (Fig. 18) can explain common features of the observations: for a low deformation, most of the *c*-axes are located on small circles whereas for a large deformation, a unique girdle oblique to the schistosity is usually observed. In this girdle, the maxima are generally not in the *XZ* plane. Due to our ignorance of the actual strain path of natural deformation, and due to the disparity of observations, more detailed comparisons with natural observations are difficult.

DISCUSSION AND CONCLUSION

It is interesting to further discuss the implications of the model proposed for the simulation. In this model, since only a few slip systems are assumed to be active, the overall deformation is heterogeneous and depends on the interaction between neighbouring cells. The numerical approach of this interaction is purely geometric and is based on the minimization of gaps, overlaps and boundary sliding. As gaps and overlaps do not exist in

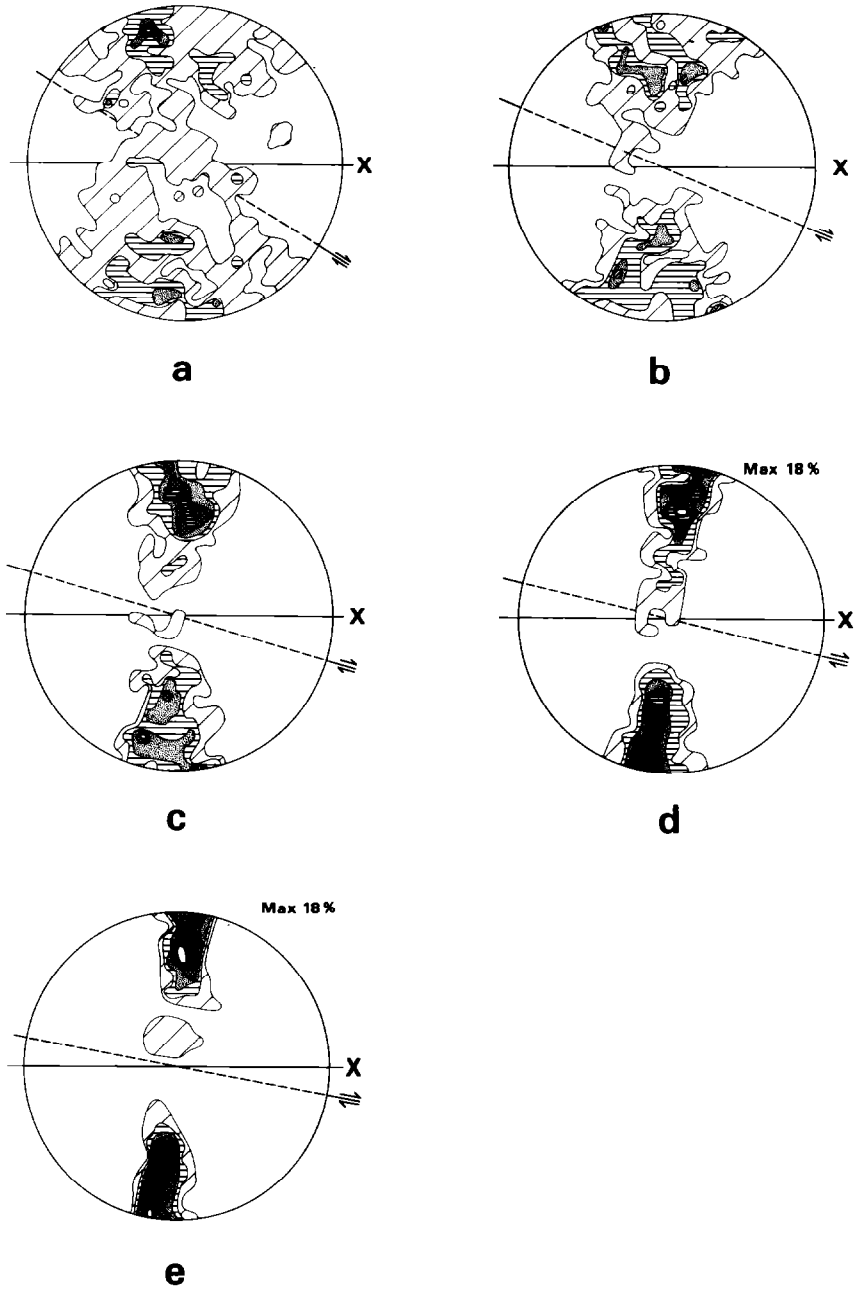

Fig. 18. Simulation of simple shear in quartz with basal and prismatic slip systems. The *c*-axis distribution is drawn for (a) $\gamma = 1$, (b) 2, (c) 3, (d) 4, and (e) 5. Isodensity contours are for 1, 3, 5, 7, 9 and 11%.

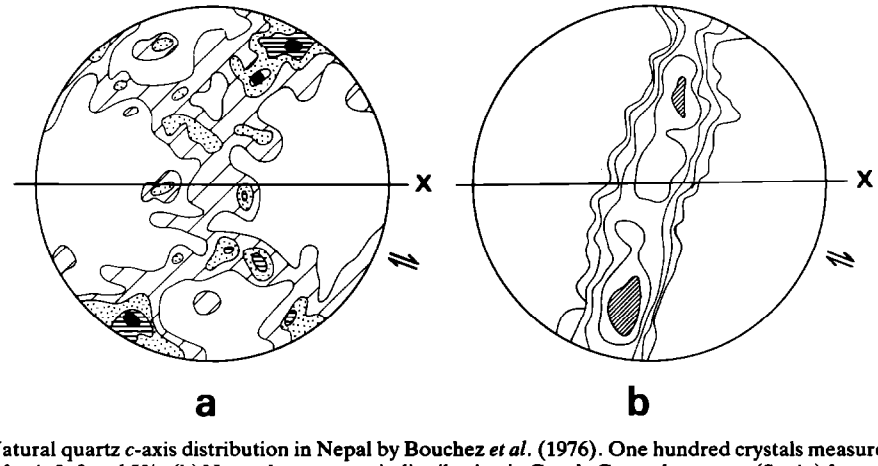

Fig. 19(a). Natural quartz *c*-axis distribution in Nepal by Bouchez *et al.* (1976). One hundred crystals measured; isodensity contours are for 1, 2, 3 and 5%. (b) Natural quartz *c*-axis distribution in Cap de Creus shear zone (Spain) from Garcia Celma (1983). 256 crystals measured; isodensity contours are for 1, 3, 5, 7 and 10%.

natural deformations, other mechanisms such as diffusion, flexuring, etc., necessarily take place in order to accommodate the deformation of each cell, but these secondary mechanisms are ignored in the model. The underlying assumption of the model is that such mechanisms are easier to activate than slip on secondary systems which are sometimes proposed to achieve a homogeneous deformation.

For large shear deformations of crystalline aggregates with dominant basal-slip systems, both this model and Lister's model fail to account for a major feature observed in experimental and natural deformation: the obliquity of *c*-axis orientations with respect to the schistosity.

The origin of these discrepancies has been discussed and, on the basis of various observations, dynamic recrystallization is proposed as an additional mechanism which becomes important for large deformation. The final result of recrystallization is the restoration of a more isodiametric shape for the various crystals. Therefore recrystallization enables external rotation of those crystals which were initially orientated in an unfavourable direction. Thus we modified our model in order to account for recrystallization; for large shear strain, our modelled LPOs then present a strong asymmetry with respect to the *XY* plane, which is consistent with the various experimental and natural observations. Another related point is that natural fabrics seem to develop more rapidly than simulated ones; such a feature can perhaps be explained by the same type of mechanisms.

The procedure for simulating the recrystallization—through complete recovery of the initial shape of each cell—is quite rough; further refinements could be introduced into the simulation but, until some physical model of recrystallization is available, such refinements would not be really informative. Again, the relative energy necessary for recrystallization to occur cannot be estimated and only the geometric results of the model can be used. The same thing is true when several slip systems can be active in each crystal.

Although very schematic, the proposed model is believed to throw some light on the develpment of Lattice Preferred Orientations during natural and experimental deformation of polycrystalline aggregates. The results of this model confirm that the general obliquity of LPO can be used as a shear criterion; on the other hand, some of the simulations show that the presence and location of maxima within the girdles are not necessarily criteria for the occurrence of secondary slip systems.

Acknowledgements—The authors acknowledge M. Brunel, J. Malavieille and D. Mainprice for fruitful discussions. They also thank D. Gapais and two referees for their pertinent remarks.

REFERENCES

Bishop, J. F. N. & Hill, R., 1951. A theory of the plastic distorsion of a polycrystalline aggregate under combined stresses. *Phil. Mag.* **42**, 414–427.

Bouchez, J. L. 1977. Plastic deformation of quartzites in an area of natural strain gradient at low temperature. *Tectonophysics* **39**, 25–50.

Bouchez, J. L. & Pécher, A. 1976. Plasticité du quartz et sens de cisaillement dans les quartzites du grand chevauchement himalayen. *Bull. Soc. géol. Fr., 7 ser.* **XVIII**, 1377–1385.

Bouchez, J. L. & Pécher, 1981. The Himalayan Main Central Thrust pile and its quartz-rich tectonites in Central Nepal. *Tectonophysics* **78**, 23–50.

Bouchez, J. L. & Duval, P. 1982. The fabric of polycrystalline ice deformed in simple shear: experiments in torsion, natural deformation and geometrical interpretation. *Textures & Microstruct.* **5**, 171–190.

Bouchez, J. L., Lister, G. S. & Nicolas, A. 1982. Fabric asymmetry and shear sense in movement zones. *Geol. Rdsch.* **72**, 401–419.

Boullier, A. M. & Nicolas, A. 1973. Texture and fabric of peridotite nodule from Kimberlite at Mothae, Thaba Putsoa and Kimberley. In: *Lesotho Kimberlites* (edited by Nixon, P. H.). Lesotho National Development Corporation, Maseru, Lesotho, 57–66.

Brunel, M. 1980. Quartz fabrics in shear-zone mylonites: evidence for a major imprint due to late strain increments. *Tectonophysics* **641**, T33–T44.

Brunel, M. 1983. Etude pétrostructurale des chevauchements ductiles en Himalaya. Unpublished thèse, Université de Paris VII.

Burg, J. P. & Laurent, P. 1978. Strain analysis of a shear zone in a granodiorite. *Tectonophysics* **47**, 15–42.

Carter, N. L., Christie, J. M. & Griggs, D. T. 1964. Experimental deformation and recrystallisation of quartz. *J. Geol.* **72**, 687–733.

Etchecopar, A. 1977. A plane kinematic model of progressive deformation in a polycrystalline aggregate. *Tectonophysics* **39**, 121–139.

Gapais, D. & White, S. H. 1982. Ductile shear band in a naturally deformed quartzite. *Textures & Microstruct.* **5**, 1–17.

Garcia-Celma, A. 1983. *c* axis and shape fabrics in quartz-mylonites of cap de Creus (Spain); their properties and development. Unpublished Ph.D. thesis, University of Utrecht.

Green, H. W., Griggs, D. T. & Christie, J. M. 1970. Syntectonic recrystallisation and annealing of quartz aggregates. In: *Experimental and Natural Rock Deformation* (edited by Paulisch, P.). Springer-Verlag, Berlin, 272–335.

Hobbs, B. E. 1968. Recrystallisation of single crystals of quartz. *Tectonophysics* **6**, 353–401.

Hudleston, P. J. 1977. Progressive deformation and development of fabric across zones of shear in glacier ice. In: *Energetics of Geological Processes* (edited by Saxena, S. & Bhattacharji, S.). Springer-Verlag, New York, 121–150.

Kojima, G., & Hide, K. 1958. Kinematic interpretation of the quartz fabric of triclinic tectonites from Besshi, Central Shikoku, Japan. *J. Sci. Hiroshima Univ.* Ser. C. **2**, 195–226.

Laurent, P. & Etchecopar, A. 1976. Mise en évidence à l'aide de la fabrique du quartz d'un cisaillement simple à déversement Ouest dans le massif de Dora Maira. *Bull. Soc. geol. Fr., 7 ser.* **XVII**, 1387–1393.

Law, R. D., Casey, M. & Knipe, R. J. 1986. Kinematic and tectonic significance of microstructures and crystallographic fabrics within quartz mylonites from the Assynt and Eriboll regions of the Moine Thrust zone N.W. Scotland. *Trans. R. Soc. Edinb.* **77**, 99–123.

Lister, G. S., Paterson, M. S. & Hobbs, B. E. 1978. The simulation of fabric development in plastic deformation and its application to quartzite: the model. *Tectonophysics* **45**, 107–158.

Lister, G. S. & Hobbs, B. E. 1980. The simulation of fabric development during plastic deformation and its application to quartzite: the influence of deformation history. *J. Struct. Geol.* **2**, 355–370.

Malavieille, J. & Etchecopar, A. 1981. Ductile shear deformation of quartzite in an Alpine crustal thrust (Ambin Massif). *Tectonophysics* **78**, 65–71.

Marjoribanks, R. W. 1976. The relation between microfabric and strain in a progressively deformed quartzite sequence from Central Australia. *Tectonophysics* **32**, 269–293.

Mattauer, M., Proust, F. & Etchecopar, A. 1977. Linéations "a" et mécanisme de cisaillement simple lié au chevauchement de la nappe des schistes lustrés en Corse. *Bull. Soc. geol. Fr., 7 ser.* **XIX**, 841–817.

Nicolas, A., Bouchez, J. L., Boudier, F. & Mercier, J. C. 1971. Textures structures and fabrics due to solid state flow in some European Lherzolites. *Tectonophysics* **12**, 55–85.

Nicolas, A., Boudier, F. and Boullier, A. M. 1973. Mechanisms of flow in naturally and experimentally deformed peridotites. *Am. J. Sci.* **273**, 853–876.

Nicolas, A. & Poirier, J. P. 1976. *Crystalline Plasticity and Solid State Flow in Metamorphic Rocks*. Wiley, London.

Prinzhofer, A. & Nicolas, A. 1980. The Bogota Peninsula, New Caledonia: a possible oceanic transform fault. *J. Geol.* **88**, 387–398.
Simpson, C. 1980. Oblique girdle orientation pattern of quartz *c*-axes from Switzerland. *J. Struct. Geol.* **2**, 243–247.
Simpson, C. & Schmid, S. M. 1983. An evaluation of criteria to deduce the sense of movement in sheared rocks. *Bull. geol. Soc. Am.* **94**, 1281–1288.
Urai, J. L., Means, W. D. & Lister, G. S. 1986. Dynamic recrystallization of minerals. In: *Mineral and Rock Deformation Studies* (the Paterson volume). *Geophysical Monograph* 36—*Am. Geophys. Union*, 167–198.
Tullis, J. A., Christie, J. M. & Griggs, D. T. 1973. Microstructures and preferred orientations of experimentally deformed quartzites. *Bull. geol. Soc. Am.* **84**, 297–314.
Von Mises, R. 1928. Mekanick der plastischen formänderung von kristallen. *Z. Angew. Math. Mech.* **8**, 161–184.

SG 9:5/6-L